14 Surface Physics

M. Hengsberger, L. Castiglioni, H.Y. Cun, L. H. de Lima, A. Hemmi, D. Leuenberger, E. Miniussi, C. Monney, Z. Novotny, C. Bernard, P. Kliuiev, A. Kostanyan, A. Schuler, R. Stania, K. Waltar, W.-D. Zabka, M. Hotz, M. Meier, H. Nussbaumer, B. Salzmann, K. von Arx, P. Dona, T. Kälin, T. Greber, and J. Osterwalder

Our laboratory is equipped for the investigation of surface and interface phenomena at the atomic level, for the preparation and characterization of clean single-crystalline surfaces, metal and molecular monolayer films, as well as sp^2-bonded single layers on surfaces. In addition, we are part of a user consortium of the soft x-ray beamline *PEARL (PhotoEmission and Atomic Resolution Laboratory)* at the Swiss Light Source. Our group has built and commissioned a compact and mobile angle-resolved photoemission (ARPES) instrument, while a second ARPES spectrometer is currently being set up together with a high-harmonic gas jet source for producing short VUV light pulses.

The research carried out during the report period can be grouped into four topics:

- 2D materials
  Monolayer hexagonal boron nitride (*h*-BN) and graphene are grown by chemical vapor deposition (CVD) on metal surfaces. We used *h*-BN on a thin film of Rh(111) in a sessile drop electrochemical cell that allowed to change the wetting angle with an electrochemical potential (cover story in Nature, June 30). The related knowledge on the electrochemical behavior is used to optimize methods for delaminating single layer *h*-BN from their metal substrate. This project is currently pursued within the European Flagship Graphene.

- Adsorbed molecular catalysts and photosensitizers
  Within the University Research Priority Program *Light to Chemical Energy Conversion* (LightChEC) we develop and study model catalyst surfaces for solar water splitting. In Section 14.1 we present results on the adsorption of Co-pyrphyrin on $Cu_2O(111)$ where the band and molecular orbital alignment appears to be particularly optimal for the charge separation process needed for photolysis of water.

- Ultrafast processes at surfaces
  This year we report on a reconstruction scheme for the recovery of the phase of molecular orbitals, in this case pentacene from angle scanned VUV photoelectron diffraction data (see Section 14.2). The nodal structure of the wave function may be reconstructed. This will serve as a tool for time resolved experiments, where the symmetry of molecular orbitals and their evolution will be studied.

- Spin shuttles
  Monolayers of endohedral Fullerenes (*spin shuttles*) like $Dy_3N@C_{80}$ order their carbon cages on surfaces. On metals they furthermore display a tendency to orient their endohedral units. Within a collaboration with the ENS Paris, the Paul Scherrer Institut and the IFW Dresden we succeeded to trace back this orientation effect to anisotropic polarization of the carbon cage that must be induced by the ionic endohedral units (see Section 14.3).

We like to highlight the award of an SNF professorship to Dr. Claude Monney, who currently has an Ambizione fellowship on "Time- and angle-resolved photoemission spectroscopy on correlated materials" in our lab.

In the following, three highlights of last year's research are presented in more detail.

14.1 Atomically resolved charge density profile in a photocatalytic p-n heterojunction

In collaboration with: Stephan Schnidrig, Benjamin Probst and Roger Alberto, Chemistry Department, Universität Zürich.

Within the University Research Priority Program *Light to Chemical Energy Conversion (LightChEC)* the group investigates model systems formed by molecular catalysts for photoinduced water splitting which are immobilized on single-crystalline oxide surfaces. The focus was set on Co-pyrphyrin, which is a porphyrin-like organometallic macrocycle that has shown a high activity for light-induced hydrogen evolution in homogeneous systems [1]. In a previous study we have characterized the adsorption behavior of pyrphyrin on Au(111) and the in-situ metalation by Co evaporation [2].

Cu_2O is a p-type semiconductor with a band gap of $2.2\,eV$ that is well suited for solar light harvesting in a photocathode. The downward band bending in the $Cu_2O(111)$ surface directs photoexcited electrons towards the surface where they can be made available for
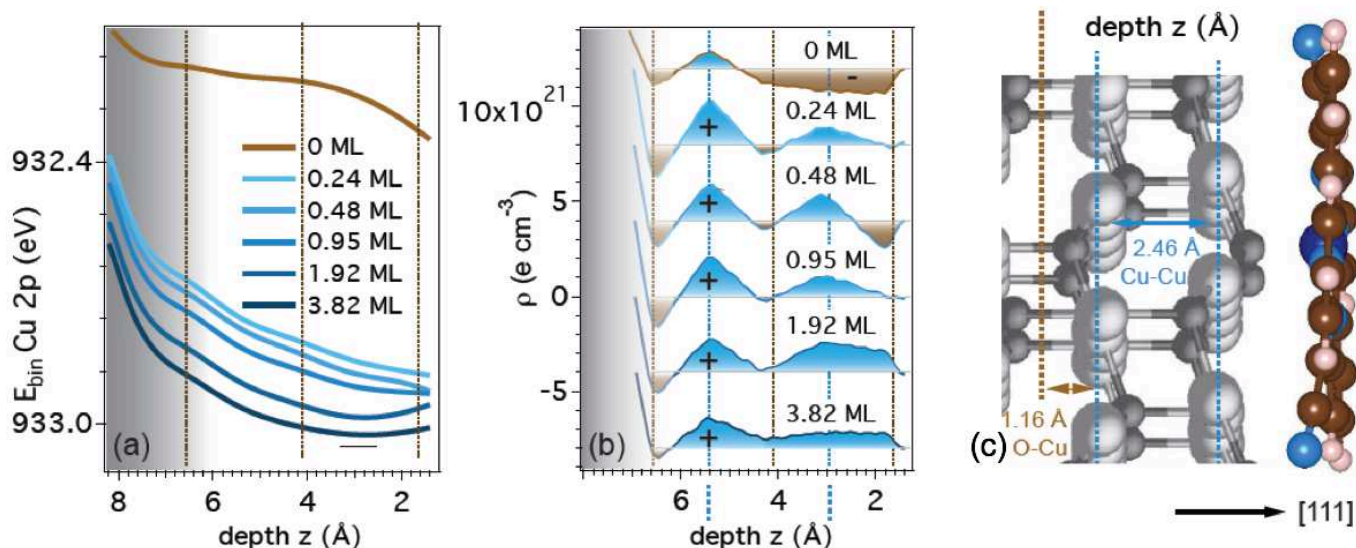
FIG. 14.1 – (a) Band bending profiles in clean and Co-pyrphyrin covered $Cu_2O(111)$ surfaces from polar-angle dependent Cu 2p core-level binding energies. The depth z represents a mean probing depth associated with a particular polar angle according to a cosine law. The different traces represent different Co–pyrphyrin coverages in units of monolayers (ML); (b) charge density profile obtained from applying Poisson's equation to the data in (a); and (c) cross sectional ball-and-stick model of the junction showing a Co-pyrphyrin molecule on the $Cu_2O(111)$ surface.

the reduction of protons via a catalyst. Measurements of the binding energies of substrate core levels by XPS can provide information on how the presence of the catalyst molecules affects the band bending.

Measurements at different photoelectron emission angles probe different depth ranges within the surface. Fig. 14.1a shows the depth dependence of the Cu 2p binding energies as a function of mean probing depth. The overall downward band bending towards the surface is readily seen, and it is conserved upon the adsorption of Co-pyrphyrin layers of various thicknesses. The observed downward offset for the molecule covered surfaces indicates an enhanced overall band bending, as these measurements show only the topmost nanometer while the band bending extends much further into the bulk of the oxide. One notices further that the curvature of the band-bending profiles close to the surface changes sign with increasing layer thickness. Moreover, slight oscillations in curvature can be observed for all curves.

Shifts in the core-level binding energies follow directly the local changes in the electrostatic potential at the position of the respective atoms. Poisson's equation relates the second derivative of the potential energy profile $V(z)$ to the local charge density profile $\rho(z)$. Corresponding curves are shown in Fig. 14.1b. Here, the oscillations are much more prominent. The maxima (positive charge) appear consistently at a distance that corresponds to the Cu-Cu layer distance (Fig. 14.1c), suggesting that the method can reveal the charge density variations with atomic resolution. On the clean $Cu_2O(111)$ surface the presence of oxygen vacancies leads to an effective negative charge on

the surface Cu atoms, while the presence of adsorbed Co-pyrphyrin molecules changes this sign. This observation can be explained by a polarization of the molecular layer in response to the electric field at the oxide surface.

[1] E. Joliat, *et al.*, Dalton Trans. **45**, 1737 (2016).

[2] G. Mette *et al.*, Nanoscale **8**, 7958 (2016).

14.2 Reconstruction of molecular wavefunctions from photoemission data

In collaboration with: Tatiana Latychevskaja (Physik-Institut, UZH), Achim Schöll (University of Würzburg, Germany); NCCR MUST.

The efficiency of molecular optoelectronic devices critically depends on charge transfer mechanisms at metal-organic interfaces. The optimization of charge transfer across interfaces thus requires rigorous time-resolved spatial visualization of these processes. A few years ago, it was shown that information about the wave functions of well-ordered organic large planar molecules on single crystalline metal substrates is encoded in angle-resolved photoelectron spectroscopy (ARPES) data [3–5]. More explicitly, the angular distribution of the photocurrent depends amongst others on the shape and phase of the initial state wavefunction.

In the case of negligible final state scattering, the final state of the photoelectron can well be approximated by a plane wave, whose momentum component parallel to the

surface plane $\vec{k}_{||}$ is preserved in the emission process:

$$\|\vec{k}_{||}\| = \sqrt{\frac{2m^\star}{\hbar^2}\left(h\nu - E_i - \phi\right)}\sin\theta,$$

where $m^\star$ denotes the effective mass of the final state, $h\nu$ the photon energy, E_i the binding energy of the initial state, ϕ the workfunction of the surface, and θ the emission angle.

Within the plane wave approximation for the photoelectron final state $\psi_f(\vec{k}) \propto \exp(\imath\vec{k}\vec{r})$, the recorded ARPES intensity distribution is related to the squared modulus of the Fourier transform of the initial state wave function $\psi_i(\vec{k})$ (the energy variables are dropped for the sake of readability) [3]:

$$I(\vec{k}_f) \propto \sum_i \sum_{\vec{k}_{i||},\vec{G}_{||}} \left|\left\langle \psi_f(\vec{k}_{f||},r)\left|\vec{A}\cdot\vec{p}\right|\psi_i(\vec{k}_{i||},r)\right\rangle\right|^2 \delta\left(\vec{k}_{f||} - \vec{k}_{i||} - \vec{G}_{||}\right)$$

$$\propto \sum_i \sum_{\vec{k}_{i||},\vec{G}_{||}} \left(\vec{A}\cdot\vec{k}_f\right)^2 \left|\underbrace{\int e^{\imath\vec{k}_{f||}\vec{r}_{||}} \psi_i(\vec{k}_{i||},\vec{r}_{||}) \delta\left(\vec{k}_{f||} - \vec{k}_{i||} - \vec{G}_{||}\right) d^2r_{||}}\right|^2$$

$$= \sum_i \left(\vec{A}\cdot\vec{k}_f\right)^2 \left|\mathcal{F}\left\{\psi_i(\vec{r}_{||})\right\}\right|^2.$$

$\vec{A}$ denotes the vector potential of the light and $\vec{G}_{||}$ a reciprocal lattice vector of the surface. The selection of the initial state i is made by choosing the corresponding peak in the energy spectrum. The angular intensity distribution of the peak intensity $I(\vec{k}_f, E_i)$ with $E_i = h\nu - E_{\text{kin}} - \phi$ thus represents the Fourier transform of $\psi_i(\vec{r}_{||})$ modulated by a slowly varying envelope function $\vec{A}\cdot\vec{k}_f$.

The initial state wavefunction $\psi_i(\vec{r}_{||})$ can be computed by inverse Fourier transform of the ARPES data, provided that the phase distribution in the detector plane is known. The phase distribution missing in the experiment may be inferred from the parity of the wave function [3], dichroism measurements [4] or iteratively, by employing knowledge about the shape of the wave function [5].

We suggest that the phase problem in ARPES based reconstruction of molecular wave functions can be solved in a more robust manner by exploiting the analogy to the phase problem in coherent diffraction imaging (CDI) [6]: provided that the far field optical intensity distribution is measured at the oversampling condition, both the amplitude and the phase of the object can be reconstructed purely from the experimentally available modulus of its Fourier transform using state-of-the-art phase retrieval algorithms, currently available in CDI [7–9]. The oversampling condition means that the ARPES image in the Fourier domain is sampled fine enough such that the ob-
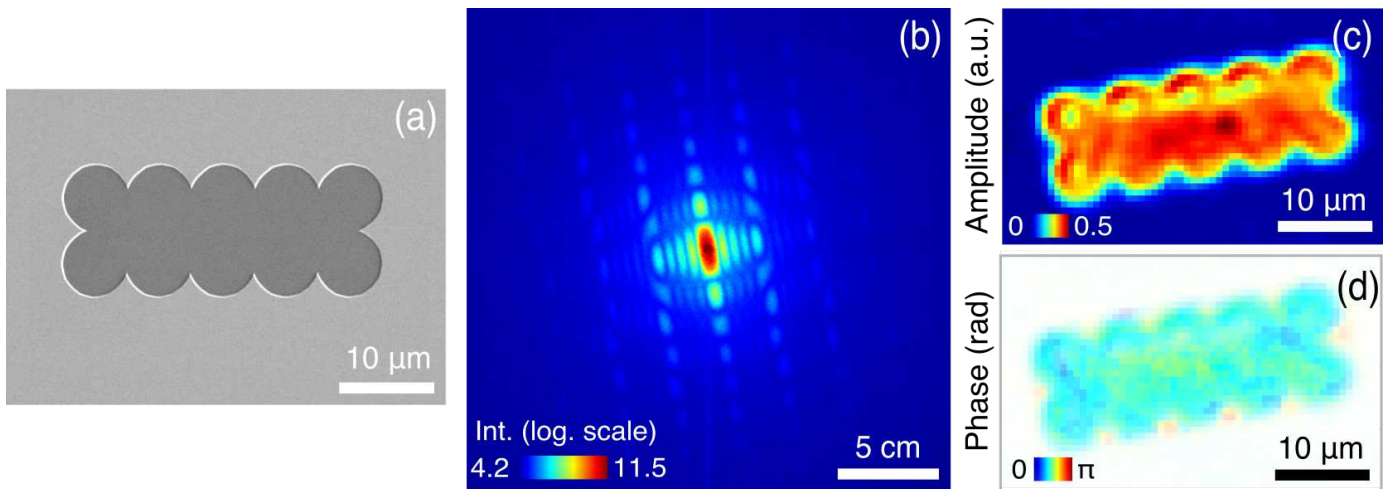

FIG. 14.2 – Results of the CDI experiment (from Ref. [10]). (a) Electron microscope picture of the pentacene orbital mimicked lithographically in Cr/SiO$_2$. (b) Diffraction pattern recorded in transmission using 532 nm laser light in normal incidence. (c) and (d) Reconstructed amplitude (c) and phase (d).
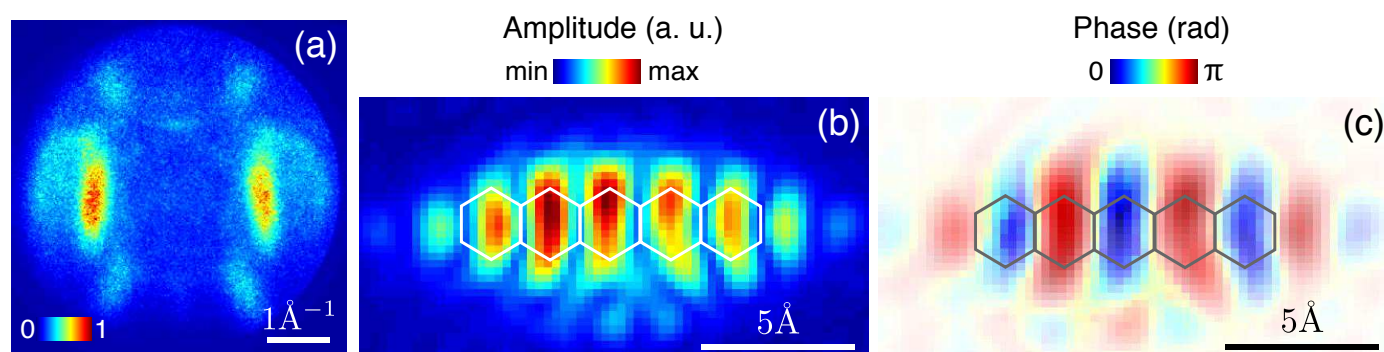
FIG. 14.3 – Reconstruction of the pentacene LUMO (from Ref. [10]). (a) Angular photoemission intensity distribution recorded using a so-called momentum microscope [11] from a sub-monolayer of pentacene on Ag(110) at a photon energy of 50 eV. (b) and (c) Reconstructed amplitude (b) and phase (c) of the LUMO. The color brightness in (c) is weighted with the corresponding amplitude values for illustration purposes.

ject distribution in real space is surrounded by a zero-padded region and the ratio between the total number of pixels in the image and the number of pixels belonging to the object exceeds two [10].

In order to demonstrate the analogy between CDI and ARPES based reconstructions, we perform an optical analogue experiment on micrometer-sized structures together with T. Latychevskaja from the group of H.-W. Fink. From the far-field diffraction patterns recorded using a 532 nm laser and a CCD camera, the amplitude and phase distributions could be reconstructed [10]. Obviously, the phase is uniform for this lithographic mimic. The ratio of the size and the laser wavelength corresponds to the ratio of the molecular orbital to the de Broglie wavelength of the photoelectrons used for the imaging of the pentacene LUMO. The results are shown in Fig. 14.2.

By applying the same algorithm to a set of ARPES data taken by the group of A. Schöll (University of Würzburg) at the Elettra Sychrotron in Trieste from an ordered sub-monolayer of pentacene molecules on Ag(110), both the amplitude and phase of the lowest unoccupied molecular orbital (LUMO) could be reproduced (see Fig. 14.3).

It has to be emphasized that no assumption on the shape or symmetry of the molecule is required as input for our algorithm. The oversampling condition is fulfilled in the present case by the length of the molecules and the resolution (pixel size) of the recorded ARPES data [10].

[3] P. Puschnig et al., Science **326**, 702 (2009).

[4] M. Wiessner et al., Nat. Comm. **5**, 4156 (2014).

[5] D. Lueftner et al., PNAS **111**, 605 (2014).

[6] J. Miao et al., Nature **400**, 342 (1999).

[7] J. Fienup, Opt. Lett. **3**, 27 (1978).

[8] S. Marchesini et al., Phys. Rev. B **68**, 140101 (2003).

[9] R. Harder et al., New J. Phys. **12**, 035019 (2010).

[10] P. Kliuiev, T. Latychevskaia, J. Osterwalder, M. Hengsberger, and L. Castiglioni, New J. Phys. **18**, 093041 (2016).

[11] C. Schneider et al., J. Elec. Spectr. Rel. Phen. **185**, 330 (2012).

14.3 Understanding the orientation of endohedral clusters in C_{80} on surfaces

In collaboration with: Ari P. Seitsonen, Département de Chimie, École Normale Supérieure, Paris, France, Matthias K. Muntwiler, Swiss Light Source, Paul Scherrer Institut, Villigen, Switzerland, and Alexey A. Popov, Nanoscale Chemistry Leibniz Institute for Solid State and Materials Research, IFW Dresden, Germany.

Endohedral Fullerenes like $TbSc_2N@C_{80}$ (Fig. 14.4a) contain isolated physical entities that are in the present case $TbSc_2N$ clusters. The carbon cage separates the endohedral from the exohedral world. This is an ideal scenario if for example magnetization shall be protected from unwanted chemical interaction. The interaction of the endohedral unit across the carbon cage is weak but finite. This is shown by the fact that different endohedral molecules like $Tb_2ScN@C_{80}$ and $TbSc_2N@C_{80}$ may be separated by high pressure liquid chromatography [12], by the observation of orientation of the endohedral units on surfaces [13], and by their magnetic ordering [14]. Although the orientation of the molecules on surfaces may be measured, and an interaction across the cage may be conjectured, [13, 14] an understanding of this effect is lacking. In combining density functional theory and electrostatics, and with comparison to experimental high-resolution x-ray photoelectron spectra we succeeded to calculate, identify and measure the interaction between the carbon cage and the ionic endohedral units. Electrostatics and concomitant polarization is im-
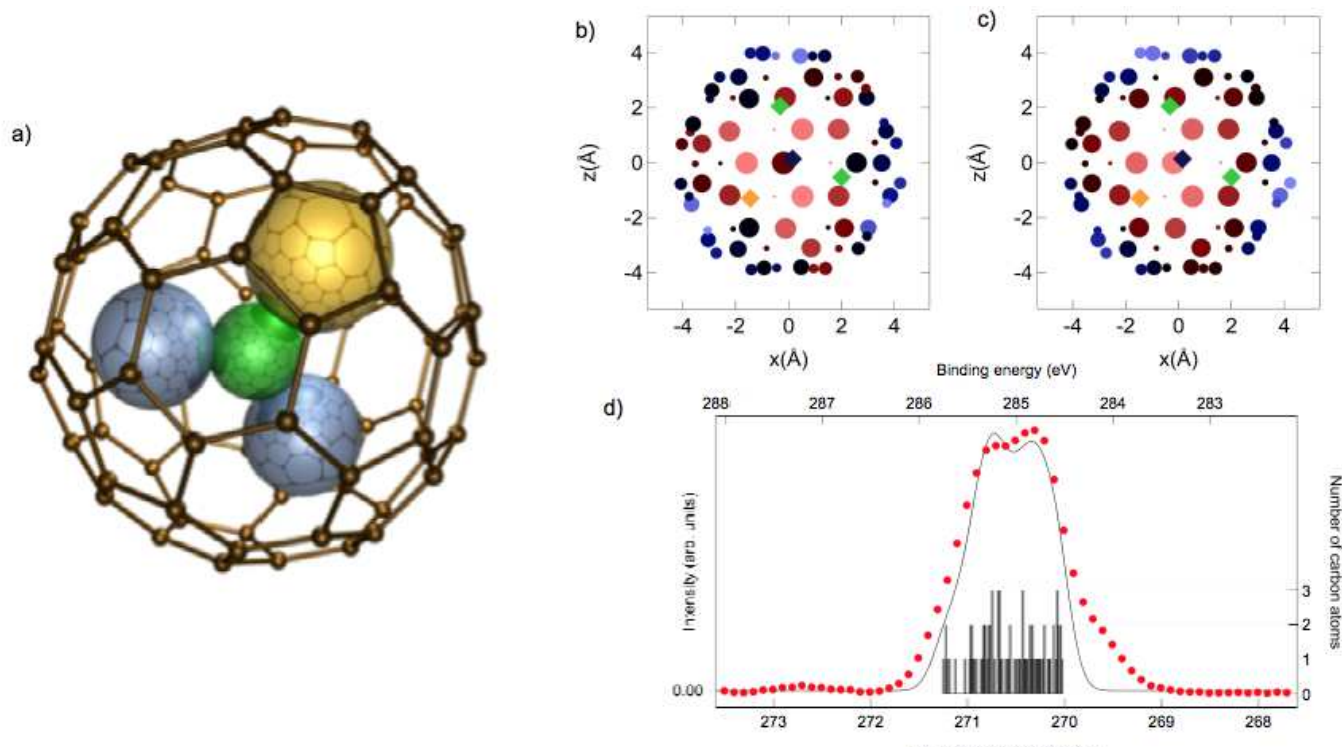
Fig. 14.4 – (a) Model of an endohedral Fullerene such as $TbSc_2N@C_{80}$. 80 carbon atoms form the cage into which fit a terbium (yellow) two scandium (light blue) and a central nitrogen atom (green). (b) C1s Density Functional Theory DFT eigenvalues (red-blue) of the 80 C atoms in $YSc_2@C_{80}$. The size of the circles represents the y-coordinate. The diamonds indicate the endohedral atoms. (c) Coulomb potential (red-blue) on the 80 C atom-sites as imposed by the endohedral ions. Note the similarity to (b). (d) Comparison of high resolution x-ray photoelectron spectroscopy (XPS) data of a submonolayer $TbSc_2N@C_{80}$ on h-BN/Ni(111) with the DFT C1s eigenvalues. The eigenvalue-spectrum (black) is convoluted and shifted to the experiment (red dots) from [15].

portant because the endohedral unit is very ionic: C_{80} is stable, if six electrons are transferred to the carbon shell. They completely fill the 8-fold degenerate highest occupied molecular orbital and stabilize it accordingly. For the case of trimetal nitride Fullerenes three trivalent rare earth atoms contribute nine electrons, where three of them fill the nitrogen 2p shell and the rest stabilizes the carbon cage.

The density functional theory (DFT) calculations of the C1s eigenvalues are shown for $YSc_2N@C_{80}$ in Fig. 14.4 b). Yttrium is isovalent to terbium and has a similar size, though may be much better handled with DFT than the open shell $4f^8$ Tb^{3+}. Theory indicates a C1s eigenvalue spectrum that is linear in the electrostatic potential, which is imposed by the ionic species inside the carbon cage. For

$TbSc_2N@C_{80}$ we observe with x-ray photoelectron spectroscopy a splitting of the C1s core level that quantitatively agrees with the splitting in the calculated DFT spectrum. This is the key fact for the understanding of chemical interaction across the Fullerene cage. These findings may be important as well for the understanding of ionic interactions across graphene or other single layer two dimensional materials.

[12] A.A. Popov, S.F. Yang, and L. Dunsch,
     Chem. Rev. **113**, 5989 (2013).

[13] M. Treier *et al.* Phys. Rev. B **80**, 081403(R) (2009).

[14] R. Westerström *et al.*
     Phys. Rev. Lett, **114**, 087201 (2015).

[15] R. Stania, PhD thesis University of Zürich 2016.